Searching for metal-poor stars

E. Caffau[1]

GEPI, Observatoire de Paris, Université PSL, CNRS, 5 Place Jules Janssen, 92190 Meudon, France e-mail: `Elisabetta.Caffau@obspm.fr`

Abstract. Metal-poor stars are fundamental objects to understand the formation and the chemical evolution of the Milky Way. They hold in their atmospheres the fossil record of the chemical composition of the early phases of the Universe so that their chemical analysis provides important constraints on the masses of the first stellar generation. Metal-poor stars are rare objects; to dig them out different techniques has been used and large amounts of data have to be processed. I will briefly summarise my experience by selecting EMP candidates from low-resolution spectroscopy, from photometry and from kinematics. I will also present the detailed chemical investigation of three stars selected from their high speed. One of these stars show the chemical peculiarities of second generation stars in globular clusters.

Key words. Stars: abundances – Stars: atmospheres – Stars: Population II – Galaxy: globular clusters – Galaxy: abundances – Cosmology: observations

1. Introduction

Metal-poor stars are stars with a metal-content well below the Solar. We usually refer to: (1) metal-poor (MP) stars when the iron content is below 1/10 the solar, $[Fe/H] < -1$; (ii) very metal-poor (VMP) stars when $[Fe/H] < -2$; (iii) extremely metal-poor (EMP) stars when $[Fe/H] < -3$ (see Beers & Christlieb, 2005, for details). This is in fact misleading because we usually associate the metallicity of the stars with iron abundance. In fact, we assume that each element X scales with iron, keeping $[X/Fe]$ constant, except for the α-elements that are enhanced in the large majority of metal-poor stars (see e.g. $[Ca/Fe] = 0.50 \pm 0.09$ in Spite et al. 2012). But we know that at metal-poor regime there are many stars extremely poor in iron but much enhanced in carbon (and other elements) with up to almost solar val-

ues, the carbon-enhanced metal-poor (CEMP) stars. The choice to scale the metallicity with iron is related to the fact that: Fe is the heaviest element that can be synthesised endothermically in stars; Fe is provided to the gas mainly by supernovae (SN) explosion, so that the highest the Fe content the larger the contribution from SN, so usually the youngest the age. But also Fe is extremely well represented in stellar spectra, being probably the easiest element to detect in the spectra of the majority of the long-lived FGK stars.

The metal-poor stars we observe at present formed from a gas cloud poorly enrich by SN explosions, so in a distant past when just few SN had the time to explode. These stars, mostly as old as the universe, with their almost unchanged chemical composition, can help us to answer questions such as: is there a critical metallicity below which low-mass stars cannot

form? What were the masses of the first stellar generation, the Pop III, stars?

Metal-poor stars are very rare objects. To find them several strategies have been put in place. Some obvious way to select good metal-poor candidates are: (a) to exploit spectroscopic database; (b) to use calibrated photometry; (c) to select stars from kinematics.

2. Spectroscopic databases

High-resolution spectroscopic surveys provide already detailed chemical abundances so there is no need for a follow-up observation to confirm the low-metallicity of a star. Follow-up observations are done just when a further element or a higher signal-to-noise ratio (S/N) are needed. The Gaia-ESO Survey (Gilmore et al., 2012) provided high-resolution spectra for more than 110 000 (see Randich et al., 2022, for details). On-going surveys, such as GALAH (De Silva et al., 2015) and APOGEE (Drory et al., 2015; Wilson et al., 2019), are providing detailed chemical abundances and are used to understand the chemical evolution of the Galaxy and the accretion events.

Low-resolution surveys are an efficient way to select good metal-poor candidates to be confirmed at high-resolution. I would like here to mention: (i) the HK Survey (Beers et al., 1985) that provided the metal-poor candidates for the ESO large programme "First Stars" (Cayrel et al., 2004); (ii) the Hamburg-ESO survey (Christlieb et al., 2000, 2008) that provided the first ultra Fe-poor star (Christlieb et al., 2002); (iii) the Large Sky Area Multi-Object fiber Spectroscopic Telescope (LAMOST Cui et al., 2012) whose metal-poor candidates have been confirmed by Li et al. (2015) and Li et al. (2022); (iv) the Sloan Digital Sky Survey (SDSS York et al., 2000) that provided several meta-poor stars (see e.g. Aguado et al., 2018).

I myself exploited the SDSS database to select metal-poor candidates, and in my project TOPoS (Caffau et al., 2013) I could confirm several extremely interesting object: the first star with [Fe/H] < −4.5 and no evidence of enhancement in carbon (Caffau et al., 2011); the only known binary SB2 system of CEMP stars

with [Fe/H] < −4.5 (Caffau et al., 2016); the discovery of two CEMP stars with [Fe/H] < −4.5 (Bonifacio et al., 2015).

3. Photometric database

Selecting metal-poor candidates from photometric databases is a wide used technique. Photometric observations provide less information than the spectroscopic ones, because their resolving power is much lower. A narrow-band filter as Pristine (Starkenburg et al., 2017), which is centred on the Ca II-H and -K lines (the strongest lines in optical spectra of FGK stars, so the most efficient to select metal-poor stars) has a resolving power of less than 40 (to be compared to about 2000 of the SDSS). Photometric observations provide the total photons in the wavelength range where the filter is transparent, but the precise wavelength information on the absorption/emission of a photon is lost. A low photon count in the band can be misinterpreted as due to low metallicity when in fact it can be due to stellar activity, which results in photon emission in the core of Ca II-H and -K lines. As an example, several metal-poor candidates selected with the Pristine filter have been confirmed to be metal-rich, active stars (see e.g. Lombardo et al. in preparation). This is why, the photometric selection of metal-poor candidates has a lower success rate than when the selection is based on low-resolution spectra, where emission lines can be identified. However, the big advantage is that photometric databases have a much larger number of objects, e.g. 110 000 targets in GES, 588 571 stars in GALAH+ DR3 (Buder et al., 2022) with respect to 1.46×10^9 sources in Gaia DR3 of which only 999 645 with an RVS spectrum (Gaia Collaboration et al., 2022) or 500 million objects in SkyMapper (Onken et al., 2019).

The combination of broad-band and narrow-band photometry revealed to be quite efficient in digging out metal-poor candidates. In fact, several stars selected in this way have been later confirmed, with spectroscopical observations, to be metal-poor stars (see e.g. Aguado et al., 2019).

This selection by using SkyMapper photometry allowed to confirm a large number of metal-poor stars (see e.g. Yong et al., 2021) and also two stars with [Fe/H] < −6 (Keller et al., 2014; Nordlander et al., 2019). The narrow-band Pristine photometry (Starkenburg et al., 2017) has been combined to wide-band photometry from SDSS, allowing to discover a very rare star with [Fe/H] < −4.5 and no evidence of enhancement in carbon Starkenburg et al. (2018). Pristine filter has also been combined to the Gaia photometric band G to select MP candidates (see e.g. Caffau et al., 2020b).

4. Selection by kinematics

It is known from long time that often high-speed stars are metal-poor (Roman, 1950), and looking at the kinematics is a technique that has ever since been used to select metal-poor stars (Beers & Christlieb, 2005; Chapman et al., 2006).

The 72 stars observed with FORS@VLT (Appenzeller et al., 1998) and analysed by Caffau et al. (2020a) with a selection by Gaia (Gaia Collaboration et al., 2018) on the transverse velocity larger than 500kms^{-1} with respect to the Sun, are in fact all metal-poor (also if none is an extreme one) with an enhancement in the α elements, as normally expected in metal-poor stars (see e.g. Cayrel et al., 2004). Several stars in this analysis showed the peculiarity to be too young for their metallicity when compared to isochrones. We concluded that this is probably a population of blue straggler stars, but with the observations at our disposal we could not exclude the unlikely existence of a young population of metal-poor stars. If these stars are confirmed to be blue straggler, the interesting question is: why blue straggler stars should have preferentially hot kinematics?

Two high-speed stars have also been selected to be observed at the Subaru telescope with the High Dispersion Spectrograph (HDS) (Noguchi et al. , 2002) and they were analysed by Matas Pinto et al. (2022). These two stars (TYC 622–742–1 and TYC 1193–1918–1) are also metal-poor (but not extreme) and α-
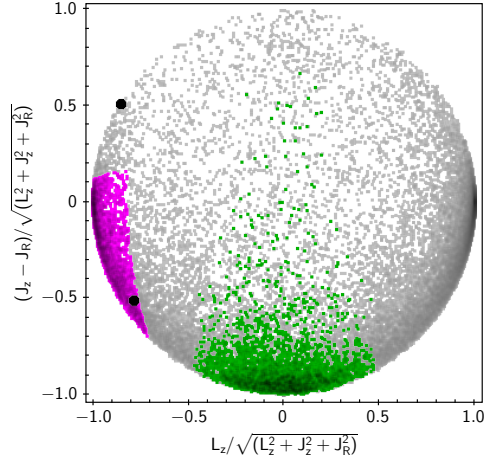
Fig. 1. The "action circle". The two black symbols are the two high-speed stars of Matas Pinto et al. (2022). The background stars: gray dots the halo TO stars from Bonifacio et al. (2021); pink dots the stars of the Sequoia accretion event; green dots Gaia-Sausage-Enceladus stars. Star TYC 1193-1918-1 has actions compatible with the Sequoia structure, while TYC 622-742-1 is neither Sequoia nor GSE, thus a "halo" star.

enhanced (metallicity of −2.37 and −1.60, respectively, see Matas Pinto et al., 2022).

When looking at the kinematics of these two stars, it results that TYC 1193–1918–1 is compatible with being part of the Sequoia accretion. To highlight it, in Fig. 1 the "action circle" is presented, that is the normalised difference between the vertical action (J_z) and the radial action (J_r) with respect to the normalised angular momentum (see Lane et al., 2022). In this representation the stars accreted to the Galaxy from a single event, such as Sequoia, cluster in a limited area of the "action circle" likely corresponding to the actions of the accreted galaxy. In the figure, the background stars are the halo turn-off stars from Bonifacio et al. (2021), I coloured in pink the stars of the Sequoia (Barbá et al., 2019) accretion event according to the definitions of Myeong et al. (2019) and in green the stars associated to the Gaia-Sausage-Enceladus (Belokurov et al., 2018; Haywood et al., 2018; Helmi et al., 2018) event according to the prescriptions of Feuillet et al. (2020).

To add statistics to the sample of stars selected for their high-speed and with detailed chemical inventory, I took the advantage of the FEROS archive to investigate three high-speed stars: CD-37 8219 (V=504 kms^{-1}), TYC 5619-109-1 (V=535 kms^{-1}) and TYC 9255-2088-1 (V=428 kms^{-1}). To show the quality of the data, in Fig. 2 the observed spectra are shown in the range of the Mg triplet.

The stellar parameters, derived in the same way as Matas Pinto et al. (2022), are listed in Table 1. In summary, the Gaia parallax, corrected by the zero-point (Lindegren et al., 2021), allowed to derive the absolute Gaia G magnitude and, with the Stefan-Boltzmann equation, the surface gravity. The effective temperature was derived by comparing the Gaia ($G_{BP} - G_{RP}$) to theoretical colours. The Gaia photometry has been dereddened by using the maps of Schlafly & Finkbeiner (2011). This process is iterative because depends on the metallicity, so that, after a first-guess metallicity, the stellar parameters are used to derive the metallicity which is then used to find new parameters. The microturbulence adopted is from the Mashonkina et al. (2017) calibration. In Fig. 3 the Gaia DR3 photometry is compared to PARSEC isochrones (Bressan et al., 2012; Marigo et al., 2017): all the stars are evolved, with CD-37 8219 and TYC 9255-2088-1 belonging to the red giant branch (RGB), while the position of TYC 5619-109-1 is less clear, compatible of being a RGB or being on the asymptotic giant branch (AGB).

The abundances have been derived by MyGIsFOS (see Sbordone et al., 2014), in the same way as described in Matas Pinto et al. (2022), with χ^2 minimisation of the observed spectrum in a selected set of metallic features on a grid of synthetic spectra computed by SYNTHE (Kurucz, 2005) by using ATLAS 12 models (Kurucz, 2005). The line-list used to compute the synthetic grid is from Heiter et al. (2021). In the lower panel of Fig. 4 the [Ca/Fe] ratio derived versus [Fe/H] is compared to literature results. The three stars are enhanced in Ca, as usually are Galactic metal-poor stars.

For the other elements, two of the stars, CD-37 8219 and TYC 9255-2088-1, show a chemical pattern similar to literature field metal-poor stars, with enhancement in α-elements. The third star, TYC 5619-109-1, the most luminous, is rich in Na, Al, enhanced in the α-elements but not in Mg (see upper panel of Fig. 4). Its Mg abundance is based on just two lines, but with a very good agreement.

In Fig. 5 the [Na/Fe] and [Al/Fe] ratios for the two stars for which these abundance could be derived, are compared to the evolved stars in the sample by Fulbright (2000). For TYC 5619-109-1, the [Al/Fe] and [Na/Fe] ratios are high, while [Mg/Fe] ratio is low ([Na/Fe]=0.47, [Al/Fe]=1.22, [Mg/Fe]=−0.09). Hayes et al. (2018) adopted different stellar parameters (4635/1.6/−1.3) for this star, but derived similar ratios.

Unfortunately, for this star the S/N in the wavelength range of the G-band is low (S/N ∼ 20) and several artifacts (emission spikes) make it difficult to derive C abundance. Anyway, the carbon abundance that could be derived is A(C) = 6.2 ± 0.3, which means [C/Fe] = −0.46. The C abundance is low because, being this star an AGB or a RGB, surely a mixed star due to the low surface gravity, it already destroyed some of its C, during the CNO cycle in the shell. The quality of the data is not sufficient to allow to derive a conclusive value on the C isotopic ratio. What can be concluded is that probably $^{12}C/^{13}C > 10$ (see Fig. 6). There is no detection of Li.

The chemical pattern of TYC 5619-109-1 seems the one of a second-generation star in a globular cluster. This pattern cannot be due to self-enrichment by the star in its AGB phase, because its mass is too low to expect a change in the Na, Mg and Al abundances (see Fig. 4 in Ventura et al., 2022). The star shows variability in radial velocity, so it could have been enriched by a now white dwarf companion in its AGB phase, but in this case the $^{12}C/^{13}C$ should be larger that the value derived.

The metal-poor star HD 201626 also has a high [Al/Fe] ratio of 1.25 (Placco et al., 2015), but this is a CEMP-s star, rich in carbon and with $^{12}C/^{13}C = 50$. Also HE 0221-2127 is rich in Al ([Al/Fe]=0.39) and not enhanced in Mg ([Mg/Fe]=0.05) (see Cohen et al., 2013), but no C and Na abundance is provided. A star more similar to TYC 5619-
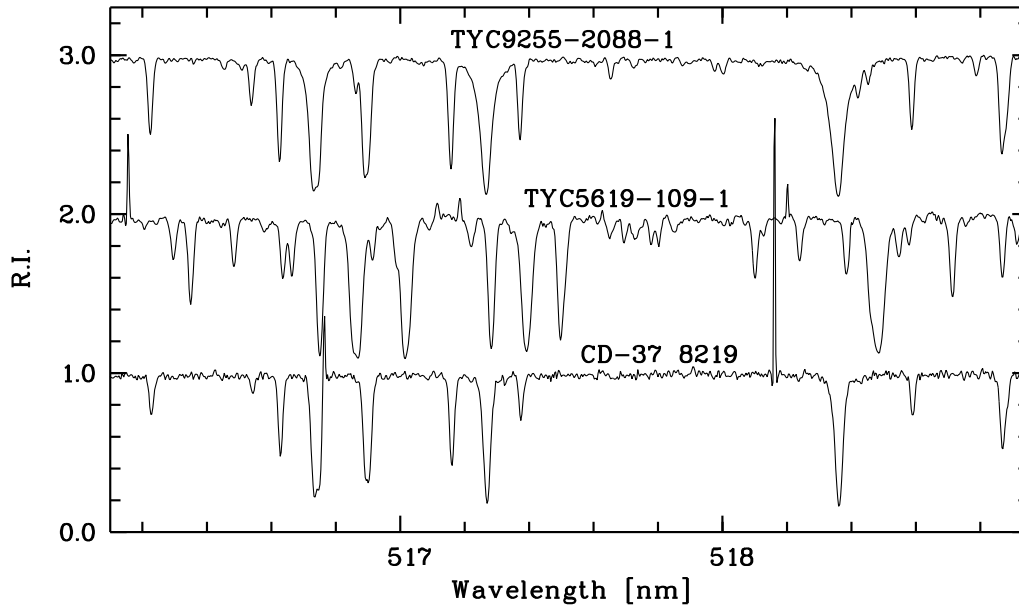
Fig. 2. The observed spectra in the range of the Mg b triplet.
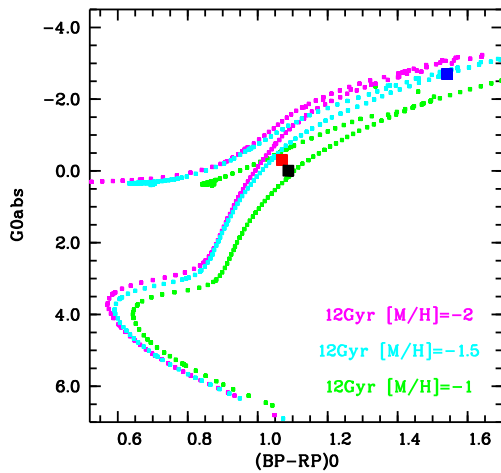
Fig. 3. The colour-magnitude diagram of the three stars here analysed as filled squares (red CD–37 8219, blue TYC 5619–1-9–1 and black TYC 9255–2088–1) compared to three PARSEC isochrones of 12 Gyr.

109-1 is HD 55496 (Pereira et al., 2019), with similar rations of [C/Fe]=–0.31, [Al/Fe]=0.76, [Na/Fe]=0.86 and $^{12}C/^{13}C = 6 \pm 1$, but a high [Mg/Fe]=0.76. Pereira et al. (2019) sug-gested this star to be a second generation star in a globular cluster, and so could also be TYC 5619-109-1.

5. Conclusions

All the methods here presented to select metal-poor stars have been proved to be efficient. Each one has a clear advantage but also limitations with respect to the others. To summarise, selecting metal-poor stars on low-resolution databases is extremely efficient, but the databases are limited in number and vice versa the selection by using photometric databases has the advantage of the huge number of objects, but the success rate is lower. The selection by kinematic is providing Halo stars, so metal-poor, but the metal-poor stars hosted in the Galactic disc cannot be selected. Also, new data available can give a hint to one of these methods, as in the case of the Gaia releases that allowed an easier and more efficient way than before to select stars on speed.

Table 1. Stellar parameters and abundances.

	CD-37 8219	TYC 5619-109-1	TYC 9255-2088-1
V_r [km/s]	176.74 ± 0.98	71.04 ± 0.85	−1.74 ± 0.61
V_rGaia [km/s]	174.22 ± 0.23	84.18 ± 0.43	−1.75 ± 0.18
T_{eff} [K]	4877	4159	4838
$\log g$	2.00	0.65	2.10
ξ [km/s]	1.77	2.01	1.66
[Fe/H]	−2.33 ± 0.13	−1.83 ± 0.19	−1.58 ± 0.13
A(O)	7.19 - 1		7.79 ± 0.07 - 2
A(Na)		4.94 ± 0.15 - 3	4.52 ± 0.11 - 4
A(Mg)	5.57 ± 0.17 - 6	5.62 ± 0.03 - 2	6.34 ± 0.14 - 5
A(Al)		5.86 ± 0.11 - 2	5.03 - 1
A(Si)	5.73 ± 0.20 - 5	6.44 ± 0.20 - 13	6.28 ± 0.08 - 19
A(Ca)	4.34 ± 0.08 - 27	4.94 ± 0.09 - 15	5.15 ± 0.05 - 25
A(Sc)II	0.94 ± 0.12 - 9	1.62 ± 0.22 - 4	1.84 ± 0.18 - 7
A(Ti)I	2.90 ± 0.21 - 30	3.44 ± 0.13 - 42	3.65 ± 0.08 - 51
A(Ti)II	2.98 ± 0.13 - 38	3.53 ± 0.11 - 15	3.76 ± 0.14 - 33
A(V)	1.74 ± 0.09 - 6	2.19 ± 0.06 - 12	2.45 ± 0.11 - 17
A(Cr)I	3.22 ± 0.08 - 14	3.89 ± 0.18 - 15	4.06 ± 0.09 - 23
A(Cr)II	3.41 ± 0.09 - 4	4.17 - 1	4.15 ± 0.25 - 8
A(Mn)	2.69 ± 0.11 - 13	3.30 ± 0.13 - 10	3.52 ± 0.04 - 15
A(Fe)II	5.29 ± 0.16 - 28	5.78 ± 0.24 - 12	5.98 ± 0.16 - 29
A(Ni)	3.92 ± 0.13 - 37	4.37 ± 0.19 - 44	4.63 ± 0.15 - 67
A(Co)	2.62 ± 0.19 - 6	3.25 ± 0.23 - 18	3.36 ± 0.14 - 22
A(Y)	−0.36 ± 0.09 - 10	0.75 ± 0.12 - 9	0.46 ± 0.14 - 12
A(Cu)		1.95 ± 0.19 - 3	2.15 ± 0.09 - 3
A(Zn)	2.30 ± 0.06 - 2	2.85 - 1	3.04 ± 0.05 - 2
A(Ba)	−0.08 ± 0.16 -3		0.81 ± 0.20 - 3

References

Aguado, D. S., Allende Prieto, C., González Hernández, J. I., et al. 2018, ApJ, 854, L34. doi:10.3847/2041-8213/aaadb8

Aguado, D. S., Youakim, K., González Hernández, J. I., et al. 2019, MNRAS, 490, 2241. doi:10.1093/mnras/stz2643

Appenzeller, I., Fricke, K., Fürtig, W., et al. 1998, The Messenger, 94, 1

Barbá, R. H., Minniti, D., Geisler, D., et al. 2019, ApJ, 870, L24. doi:10.3847/2041-8213/aaf811

Beers, T. C. & Christlieb, N. 2005, ARA&A, 43, 531. doi:10.1146/annurev.astro.42.053102.134057

Beers, T. C., Preston, G. W., & Shectman, S. A. 1985, AJ, 90, 2089. doi:10.1086/113917

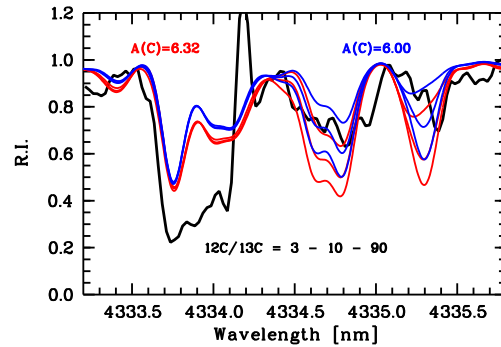Belokurov, V., Erkal, D., Evans, N. W., et al. 2018, MNRAS, 478, 611. doi:10.1093/mnras/sty982
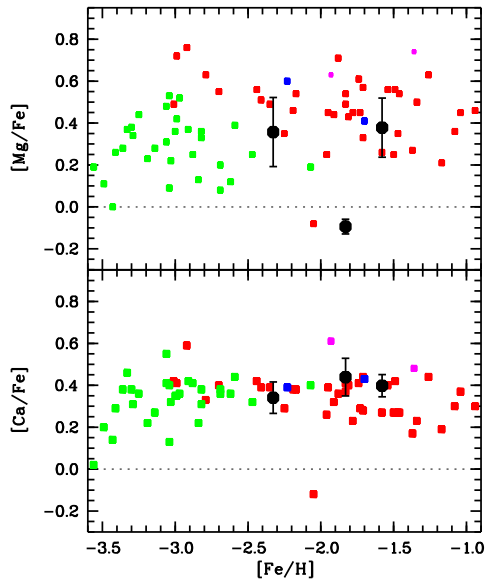
Fig. 4. [Mg/Fe] and [Ca/Fe] vs. [Fe/H] for the stars here analysed (black dots) in comparison to literature results: Cayrel et al. (green squares 2004), Fulbright (red squares 2000), Valentini et al. (pink squares 2019), Matas Pinto et al. (blue squares 2022).
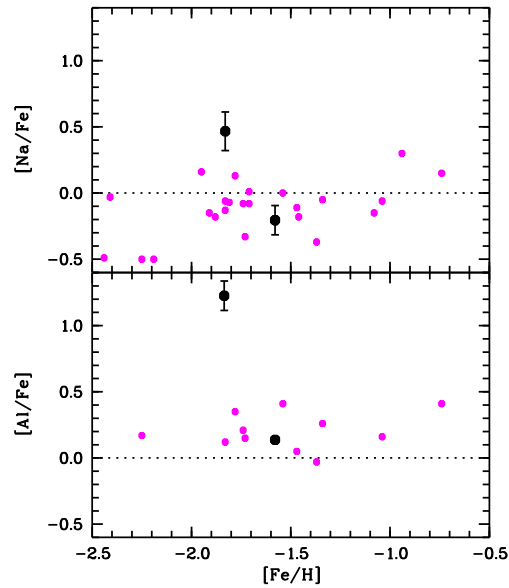
Fig. 5. [Na/Fe] and [Al/Fe] vs. [Fe/H] for two stars here analysed (TYC 5619-109-1 and TYC 9255-2088-1, black dots) in comparison results by Fulbright (2000).

Fig. 6. TYC 5619-109-1 (solid black) in the G-band range. Over-plotted: synthetic spectra with two A(C) values and three $^{12}C/^{13}C$ ratios.

Bonifacio, P., Monaco, L., Salvadori, S., et al. 2021, A&A, 651, A79. doi:10.1051/0004-6361/202140816

Bonifacio, P., Caffau, E., Spite, M., et al. 2018, A&A, 612, A65. doi:10.1051/0004-6361/201732320

Bonifacio, P., Caffau, E., Spite, M., et al. 2015, A&A, 579, A28. doi:10.1051/0004-6361/201425266

Bressan, A., Marigo, P., Girardi, L., et al. 2012, MNRAS, 427, 127

Buder, S., Lind, K., Ness, M. K., et al. 2022, MNRAS, 510, 2407. doi:10.1093/mnras/stab3504

Caffau, E., Monaco, L., Bonifacio, P., et al. 2020, A&A, 638, A122. doi:10.1051/0004-6361/202038057

Caffau, E., Bonifacio, P., Sbordone, L., et al. 2020, MNRAS, 493, 4677. doi:10.1093/mnras/staa589

Caffau, E., Bonifacio, P., Spite, M., et al. 2016, A&A, 595, L6. doi:10.1051/0004-6361/201629776

Caffau, E., Bonifacio, P., Sbordone, L., et al. 2013, A&A, 560, A71. doi:10.1051/0004-6361/201322488

Caffau, E., Bonifacio, P., François, P., et al. 2011, Nature, 477, 67. doi:10.1038/nature10377

Cayrel, R., Depagne, E., Spite, M., et al. 2004, A&A, 416, 1117. doi:10.1051/0004-6361:20034074

Chapman, S. C., Ibata, R., Lewis, G. F., et al. 2006, ApJ, 653, 255. doi:10.1086/508599

Christlieb, N., Schörck, T., Frebel, A., et al. 2008, A&A, 484, 721. doi:10.1051/0004-6361:20078748

Christlieb, N., Bessell, M. S., Beers, T. C., et al. 2002, Nature, 419, 904. doi:10.1038/nature01142

Christlieb, N., Reimers, D., Wisotzki, L., et al. 2000, The First Stars, 49. doi:10.1007/10719504_6

Cohen, J. G., Christlieb, N., Thompson, I., et al. 2013, ApJ, 778, 56. doi:10.1088/0004-637X/778/1/56

Cui, X.-Q., Zhao, Y.-H., Chu, Y.-Q., et al. 2012, Research in Astronomy and Astrophysics, 12, 1197. doi:10.1088/1674-4527/12/9/003

De Silva, G. M., Freeman, K. C., Bland-Hawthorn, J., et al. 2015, MNRAS, 449, 2604. doi:10.1093/mnras/stv327

Drory, N., MacDonald, N., Bershady, M. A., et al. 2015, AJ, 149, 77. doi:10.1088/0004-6256/149/2/77

Feuillet, D. K., Feltzing, S., Sahlholdt, C. L., et al. 2020, MNRAS, 497, 109. doi:10.1093/mnras/staa1888

Fulbright, J. P. 2000, AJ, 120, 1841

Gaia Collaboration, Brown, A. G. A., Vallenari, A., et al. 2018, A&A, 616, A1

Gaia Collaboration, Vallenari, A., Brown, A. G. A., et al. 2022, arXiv:2208.00211

Gilmore, G., Randich, S., Asplund, M., et al. 2012, The Messenger, 147, 25

Hayes, C. R., Majewski, S. R., Shetrone, M., et al. 2018, ApJ, 852, 49. doi:10.3847/1538-4357/aa9cec

Haywood, M., Di Matteo, P., Lehnert, M. D., et al. 2018, ApJ, 863, 113. doi:10.3847/1538-4357/aad235

Heiter, U., Lind, K., Bergemann, M., et al. 2021, A&A, 645, A106. doi:10.1051/0004-6361/201936291

Helmi, A., Babusiaux, C., Koppelman, H. H., et al. 2018, Nature, 563, 85. doi:10.1038/s41586-018-0625-x

Keller, S. C., Bessell, M. S., Frebel, A., et al. 2014, Nature, 506, 463. doi:10.1038/nature12990

Kurucz, R. L. 2005, Memorie della Societa Astronomica Italiana Supplementi, 8, 14

Lane, J. M. M., Bovy, J., & Mackereth, J. T. 2022, MNRAS, 510, 5119. doi:10.1093/mnras/stab3755

Li, H.-N., Zhao, G., Christlieb, N., et al. 2015, ApJ, 798, 110. doi:10.1088/0004-637X/798/2/110

Li, H., Aoki, W., Matsuno, T., et al. 2022, ApJ, 931, 147. doi:10.3847/1538-4357/ac6514

Lindegren, L., Klioner, S. A., Hernández, J., et al. 2021, A&A, 649, A2. doi:10.1051/0004-6361/202039709

Marigo, P., Girardi, L., Bressan, A., et al. 2017, ApJ, 835, 77

Mashonkina, L., Jablonka, P., Pakhomov, Y., et al. 2017, A&A, 604, A129

Matas Pinto, A. del M., Caffau, E., François, P., et al. 2022, Astronomische Nachrichten, 343, e10032. doi:10.1002/asna.20210032

Myeong, G. C., Vasiliev, E., Iorio, G., et al. 2019, MNRAS, 488, 1235. doi:10.1093/mnras/stz1770

Noguchi, K., Aoki, W., Kawanomoto, S. et al. 2002, PASJ54, 855

Nordlander, T., Bessell, M. S., Da Costa, G. S., et al. 2019, MNRAS, 488, L109. doi:10.1093/mnrasl/slz109

Onken, C. A., Wolf, C., Bessell, M. S., et al. 2019, PASA, 36, e033. doi:10.1017/pasa.2019.27

Pereira, C. B., Drake, N. A., & Roig, F. 2019, MNRAS, 488, 482. doi:10.1093/mnras/stz1411

Placco, V. M., Beers, T. C., Ivans, I. I., et al. 2015, ApJ, 812, 109. doi:10.1088/0004-637X/812/2/109

Randich, S., Gilmore, G., Magrini, L., et al. 2022, arXiv:2206.02901

Roman, N. G. 1950, ApJ, 112, 554

Sbordone, L., Caffau, E., Bonifacio, P., & Duffau, S. 2014, A&A, 564, A109

Schlafly, E. F. & Finkbeiner, D. P. 2011, ApJ, 737, 103. doi:10.1088/0004-637X/737/2/103

Spite, M., Andrievsky, S. M., Spite, F., et al. 2012, A&A, 541, A143. doi:10.1051/0004-6361/201218773

Starkenburg, E., Aguado, D. S., Bonifacio, P., et al. 2018, MNRAS, 481, 3838.

doi:10.1093/mnras/sty2276

Starkenburg, E., Martin, N., Youakim, K., et al. 2017, MNRAS, 471, 2587. doi:10.1093/mnras/stx1068

Valentini, M., Chiappini, C., Bossini, D., et al. 2019, A&A, 627, A173

Ventura, P., Dell'Agli, F., Tailo, M., et al. 2022, Universe, 8, 45. doi:10.3390/universe8010045

Wilson, J. C., Hearty, F. R., Skrutskie, M. F., et al. 2019, PASP, 131, 055001. doi:10.1088/1538-3873/ab0075

Yong, D., Da Costa, G. S., Bessell, M. S., et al. 2021, MNRAS, 507, 4102. doi:10.1093/mnras/stab2001

York, D. G., Adelman, J., Anderson, J. E., et al. 2000, AJ, 120, 1579